Engineering Physics
2024; Vol. 7, No. 1, pp. 1-9
https://doi.org/10.11648/j.ep.20240701.11

Research Article

Calculations of Stopping Power, Straggling and Range Projected of $FeKr^+$

Mohamed Farjallah*

Electronic Department, Higher Institute of Applied Sciences and Technology of Sousse, University of Sousse, Sousse, Tunisia

Abstract

The present work consists of the simulation of the interaction of a beam of Kr^+ ions with a solid iron target by the software SRIM (Stopping and Range of Ions In Matter). Our goal is to calculate different parameters related to sputtering and ion implantation in a target, such as the spatial distribution of implanted ions, the distributions of electronic and nuclear energy losses as a function of penetration depth and sputtering efficiency, as well as the damage created inside the target. The sputter induced photon spectroscopy technique was used to study the luminescence spectra of the species sputtered from Iron powder, during 5 keV Kr^+ ions bombardment in vacuum better than 107 torr. The optical spectra recorded between 350 and 470 nm exhibit discrete lines which are attributed to neutral excited atoms of Iron (Fe). The experiments are also performed under 105 torr ultra-pure oxygen partial pressure. To ensure the maximum efficiency of molecular modification process, energy of irradiation was decided by using of SRIM software. Based on SRIM simulation of Iron ions interaction with Krypton, the areas on which effect of high energy ions will maximum were predicted. A comparative analysis of molecular before and after irradiation was carried out by scanning electron microscopy. The maximum change in Krypton morphology, in the form of destruction of walls, was appeared at a distance of about μm from the start point of Fe^+ ions track inside the molecular. A substantiation of reason of wall degradation in this area was proposed.

Keywords

SRIM 2013 Software, Stopping Power, Range Projected

1. Introduction

Since its inception a century ago [1-3], the stopping power and energy dissipation of charged particles through matter has piqued attention due to its numerous applications, including radiology, ion implantation, nuclear physics, fundamental particle physics, and radiation damage. Atomic excitation and ionization are the main ways that heavy charged particles moving through materials lose energy [4]. As the mean energy loss per unit path length -dE/dx the stopping power is determined. Naturally, the target material is a factor as well as the projectile's charge and velocity [5, 6]. A generic stopping power formula [6] is obtained from early studies of the energy loss of charged particles moving through materials. Ion beams lose energy when they collide with target nuclei (nuclear stopping) and electrons (electronic stopping) when they pass through matter [7]. The stopping power resulting from nuclear and electrical interactions then adds up to the overall stopping

*Corresponding author: farjallah_mohamed@yahoo.fr (Mohamed Farjallah)

Received: 6 March 2024; **Accepted:** 27 March 2024; **Published:** 17 May 2024

Copyright: © The Author(s), 2024. Published by Science Publishing Group. This is an **Open Access** article, distributed under the terms of the Creative Commons Attribution 4.0 License (http://creativecommons.org/licenses/by/4.0/), which permits unrestricted use, distribution and reproduction in any medium, provided the original work is properly cited.

power [8, 9]. Electronic stopping power is typically used to characterize the overall energy loss at low energies [10]. It is also possible to overlook the nuclear portion of the stopping power [7]. The potential phenomena that could be responsible for the electronic stopping in the velocity area that is significantly lower than the speed of light [9].

How ions and other highly charged particles, such as alpha particles, interact with matter will be examined in this work. Additionally, how these interactions affect the human body, will be demonstrated, including the skin, bones, skeleton, and various bodily components. The relationship between energy loss and dose simplifies the formulation of how matter interacts with internal and exterior radiation to forecast the radiation treatment's affectivity as well as potential harm to nearby biological tissue. A person receiving radiation therapy is subject to various radiation types and their interactions with matter (body tissue) [9], energy loss, and doses to which they may be exposed while receiving medical care or in an accident. In numerous fields of research and application, including radiation dosimetry, radiation biology (including cell lethality, cytogenesis changes, mutagenesis, and DNA recombination), radiation chemistry, radiotherapy, and nuclear physics, the stopping power, energy loss, range, straggling, and equivalent dose rate of ions in air, tissue, and polymers are critical [11, 12]. Indirect verification of the stopping power based on alpha energy losses in air, self-supporting method, gamma resonance shift measurements, backscattering from thick substrate covered with deposited absorbing layers, direct energy loss measurement through films, and other methods have all been reported for measuring the stopping power of charged particles [2-7]. Numerous theoretical and practical investigations concerning energy loss, range, stopping power, and straggling of ions (H, He, Li, C, O), as well as similarities. As a result of the above external and internal radiation interactions with matter, the main goal is to calculate the energy loss per distance, or the stopping power and ranges that result. This will enable assessments of energy loss and doses, which are crucial for radiation therapy and the potential harm to nearby body tissue. It is common knowledge that tissue ionization values correlate with cell damage. Thus, this study's primary goal is to assess the energy deposition of helium ions in the target organ and its numerous entrance layers, which include the skin, water, adipose tissue, muscle skeletal structure, and bone. For these calculations, the SRIM 2008 code [11, 12] will be utilized, as well as the Pstar, Astar, and Estar codes [16]. The energy that ranges between 10 Kev and 10 MeV are used, and the stopping power are computed using the Bethe-Bloch formula as given in the theory of [13]. SRIM tables of stopping power, linear energy transfer (LET), and projected range (R) versus particle energy have been used in this study using the SIRM 2008 code. These tables are very helpful for the computation of particle transport in a variety of simulation applications that do not directly involve an ion transport code. The following function for fitting is utilized in order to simulate the linear energy transfer provided by SRIM tables in the specified energy range, even though a unique independent executable program (SRIM Module.exe) can be employed as a subroutine for Windows applications [17].

For example, [18-20] highlight the many unique features of nanostructures that make them very motivating. It is possible to create nanostructures with preset sizes and forms using the template synthesis approach [21]. For the persistence of generating templates grounded on silicon [25], polymer films [26], and oxide materials like Al_2O_3 [27], TiO_2 [28], and SiO_2 [29], other less common techniques such as lithography [23], anodizing [24], and ion-track technology [22] can be employed. Electrochemical deposition is commonly exploited to fill the pores; nanowires and nanotubes are mostly designed giving to the geometric features of the template openings. Some potential benefits of nanotubes over nanowires include their greater specific surface area [31] and lower specific gravity [30]. Additionally, because magnetic nanotubes lack a magnetic core, it is possible to produce nanostructures with uniform switching fields [32]. By irradiating them with high-energy ions, nanomaterials can be changed to acquire new features. This effect permits alteration of the electrical, optical, and magnetic characteristics in addition to the structure [33]. Both nuclear energy losses (<1 MeV/nucleon) and electron energy losses (dE/dx) (>1 MeV/nucleon) are the two ways that ions' energy is transported in the target material [34, 35]. Mainly, the mass, energy, and fluence of the incident ions determine the creation of defects [36]. Contingent on the regime, an ion beam can utilize implantation or irradiation to change the characteristics of nanostructures in practically all nanomaterials [37]. Notably, the free program SRIM can be used to simulate the processes complicated in adjusting nanostructures using ion radiation with the highest possible efficiency. High and low energy works in number [38] the structure, composition, and electrophysical characteristics of the irradiated nanowires in the polymer template are discussed in the publication on ions irradiation of nanowires. Also observed at fluences up to 1013 cm^{-2} is a shift in conductivity type from metallic to semiconductor [39]. Unfortunately, the process of irradiation can cause structural destruction of nanoobjects in addition to changing their characteristics. Through modeling of ions' interaction processes with target material, it is feasible to identify locations of nanostructures where most damage will occur. In this homework, the relationship between the SRIM-modeled required energy and the regions where high-energy ion effects are greatest is demonstrated using an example of irradiating Ni nanotubes with carbon ions.

2. Theory and Computational Details

The outcomes of the study's simulations, which included calculating stopping powers, varying moment distributions of different ions, energy losses, and erosion rate under ion bombardment in an iron target, will be presented in this article. The tool of choice for doing this kind of computation was the

SRIM software, which is available for free. Various simulations (SRIM, version 2013) are run once the calculating software is presented to ascertain the impact of the various implantation parameters used in this investigation.

Monte-Carlo methods [40] are employed, which include the SRIM tool, to compute damage energy distributions.

Utilizing the approximation of binary collisions and the Monte Carlo method as its foundation, the simulations were performed using the SRIM 2013 software (Stopping and Range of Ions in Matter). This software is a collection of Windows-based tools that allow one to model both the trajectory of recoiling atoms in a solid and the trajectory of an ion at incidence energies between 10 eV and 2 GeV [41, 42]. The three primary programs are the stopping power of ions computation (Stopping/Range Tables) and the detailed calculation (TRIM computation), both of which have an easy-to-use interface. In the initial program, the manipulator will be guided to an interface where it will be asked to enter two types of data: the target (Target) and the ion (type, energy range).

This paper is organized as follow. In section 2, the used methodology is briefly presented. The results for $FeKr^{+}$ are reported and discussed in Section 3. Finally, a conclusion is given in section 4.

3. Results and Discussion

Simulation of Stopping Powers in the Target

The stopping powers, energy losses, energy distribution variations, and rate of erosion under ion bombardment in an iron target are all examples of the consequences of the study's simulations, which it will discuss in this article. the device of choice for doing this computation was the open-source Monte-Carlo program SRIM. Various simulations (SRIM, version 2008) are run once the calculating software is presented in order to determine the impact of the various implementation parameters of this investigation.

The many moments of the distributions produced by the SRIM software as well as the simulation results of the systems' various stopping powers (nuclear and electronic) will be shown in this section.

Both nuclear and electrical interactions cause the ions that are attacking the target to slow down. As a beam of Kr^{+} ions cooperate with an iron target, Figure 1 illustrates how the electronic stopping power and nuclear stopping power change according to the input particle's energy. A distinction is seen between the evolution of the electronic and nuclear stopping power based on the curves provided by the SRIM software. The nuclear slowing is larger than the electronic slowdown at low energy (E < 100 keV), and this elastic interaction creates a collision cascade that displaces atoms in the target. Nuclear energy loss occurs at very low energies and grows rapidly; at higher energies, the rate of loss decreases. Regarding the electronic stopping power, it's in good accord with the LSS (Lindhard, Scharff, and Schiott) hypothesis [43], which states that it's proportional to both the incident energy and the square root (see Figure 1).

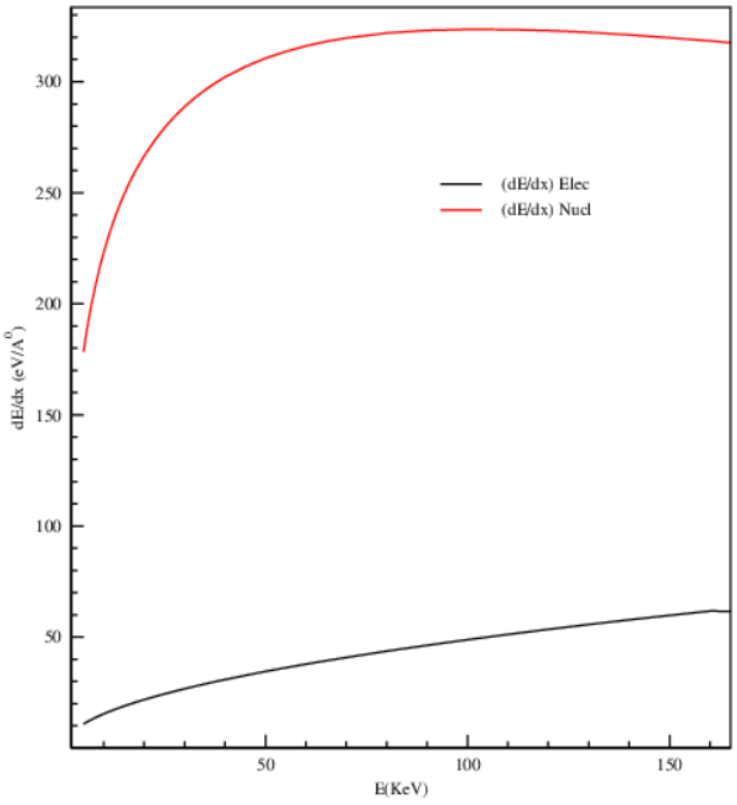

Figure 1. *Simulation of the stopping powers (nuclear and electronic) of Kr^{+} ions in an Fe target.*

When considering the system in the energy interval [0-200keV], the electronic stopping power grows almost linearly with the incident ion's energy. As a function of the reduced parameters (ε and ρ), this is reliable with the linear progress of the decreased electronic stopping power provided by the L. S. S theory. The nuclear stopping power for a particular ion (Kr^{+}) is shown by the curve to be essentially constant throughout the energy interval under consideration. It is remarkable that this nuclear stopping power rises with incident ion mass.

The next results will be devoted to ions with low velocities up to 200 keV. To provide more detail on the stopping power design, a comparison of the various corrections employed in SRIM is first presented. Next, a tabulation of the ions' projected and straggling ranges at the three energies mentioned above is done. The diverse angle yields for ion energies of 0 keV, 50 keV, and 200 keV will then be investigated using the TRIM results. Ultimately, the same simulation is run to inspect the conveyed ions' energy spectrum at various angles of leaving and target widths of iron.

The various moments of the distributions produced by the SRIM software as well as the simulation results of the systems' various stopping powers (nuclear and electronic) will be shown in this section. The system (Kr) in an iron (Fe) target with an energy between [5 and 200 keV] is shown in Table 1 that was produced by SRIM. In order to investigate how energy affects the stopping powers and moments of the ion distributions (Kr) on the Iron (Fe) target, the ions' energy are changed within the range of [50 to 200 keV]. Regarding the five systems, an approximately linear increase is seen in the electronic stopping power with incident ion energy within the energy interval [50-200keV]. The L.S.S theory's reduced electronic stopping power, evaluated as a function of the reduced parameters, shows a linear progression that aligns with this value.

This indicates that mass and energy have a linear effect on moments. The curves that show the variations of the moments R_P, ΔR_p, and σ_p of the incident ion distributions Kr in Iron in the energy interval [50 to 200 keV] follow the same trend, i.e., a practically linear evolution.

Table 1. *Groups the results of the Kr system in Fe.*

The energy of the Kr ion (keV)	Electronic stopping power (eV/Å)	Nuclear stopping power (eV/Å)	Longitudinal deviation ΔRp (Å)	Lateral deviation σ_p (Å)
50,00	$3{,}451E^{+01}$	$3{,}106E^{+02}$	62	45
100,00	$4{,}881E^{+01}$	$3{,}236E^{+02}$	101	73
150,00	$5{,}977E^{+01}$	$3{,}198E^{+02}$	137	99
200,00	$4{,}702E^{+01}$	$3{,}115E^{+02}$	174	124

All other implantation parameters are fixed in order to investigate how the angle of incidence of the ion beam affected the rate of erosion in an Iron Fe target. The Kr ion was selected for this, its energy set at 5 keV, the target depth set at 300 A°, and the angle of incidence (θ) varied from 0 to 90° (see to table 2).

Table 2. *Values of the erosion rate as a function of the angle of incidence (θ) for the Kr system at 5 keV in Fe.*

θ	**0 °**	**10 °**	**20 °**	**30 °**	**40 °**	**50 °**
Erosion rate	1,25	1,27	1,69	2,46	3.69	5,66

θ	**60 °**	**70 °**	**80 °**	**83 °**	**85 °**	**90 °**
Erosion rate	8,83	14,1	18,87	18,33	16;96	10,11

The moments of the ion distributions (Kr) in the Fe target within the energy range of [0 to 200 keV] are gathered in Figure 2. The curves that display the changes in the moments of the incident Kr ion distributions in iron throughout the

energy range of 0 to 200 keV exhibit a nearly linear evolution, which is consistent with the trend. The ion's mass variation also exhibits a linear evolution, indicating the linear influence of both mass and energy on the moments.

In the energy interval [0 to 200 keV], curves 2 and 3 that represent the fluctuations in the moments of the distributions of the incident Kr+ ions in iron follow a nearly linear evolution; the evolution of the ion's mass remains consistent. this observes the moments' linear relationship with energy and mass.

For the default density at STP and the lowest density that can be reached through SRIM before it rounds down to zero, the straggling and range have been summarized in figures 2 and 3 in order to verify the proportionality of density with the projected ranges of ions in matter. With a target depth of 2 cm, TRIM was used to collect all values for Fe ions in Kr. As energy levels drop, range generally does as well.

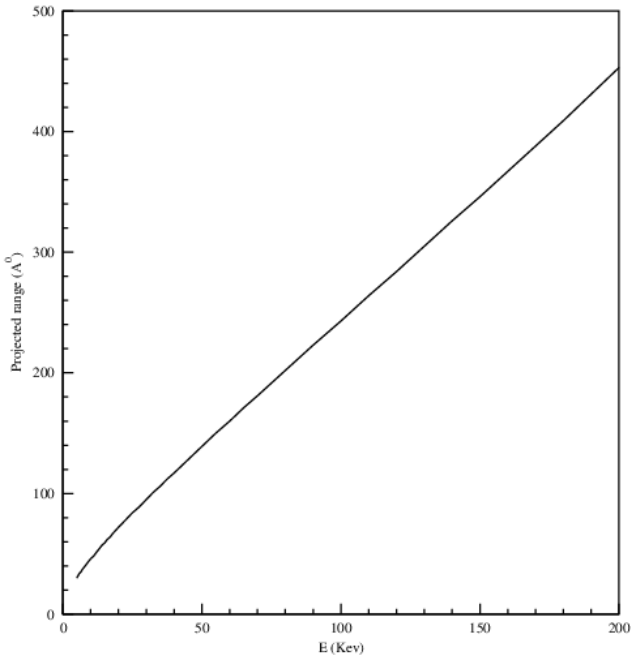

Figure 2. *The evolution of the projected range of ions (Kr) in an Fe target as a function of energy in the interval [0 to 200 keV].*

Generally speaking, the depth scale at each ion energy and other uncertainties associated with the ToF-SIMS characterisation could be impacted by surface roughness and chemical compositions [43, 44]. A large sample depth of each resist data by Kr+ cluster in the TS test may induce smearing of the depth scale. As a result, the signal intensities of nearby sample depths overlap. Therefore, in order to look at the absolute values of the characteristic depths for various ion energies, more depth calibration is required. Program SRIM (The Stopping and Ranges of Ions in Matter) [45] was used to simulate the ion range as a function of ion energy, as illustrated in Figure 4, in order to compare the ion ranges of the Kr+ ions in the surface layer of the resist for different ion energies. Keep in mind that the simulation, which displays a resist result akin to the one obtained, utilizes the PMMA values stored in the SRIM program. The Kr^+ ion range at ion energy in eV is displayed in Figure 4 for the resist surface layer. In terms of unit volume (ions/cm^3) and unit implantation dosage (ions/cm^2), it corresponds to a typical depth profile of the concentration of Kr+ ions in resist. Before decreasing with goal dep, the concentration of Kr+ ions first rises to its maximum.

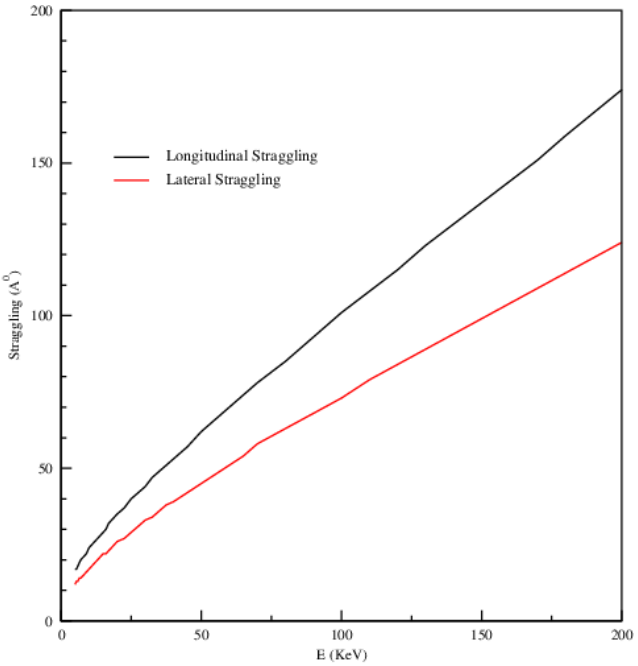

Figure 3. *The longitudinal evolution of ions (Kr) in an Fe target as a function of energy in the interval [0 to 200 keV].*

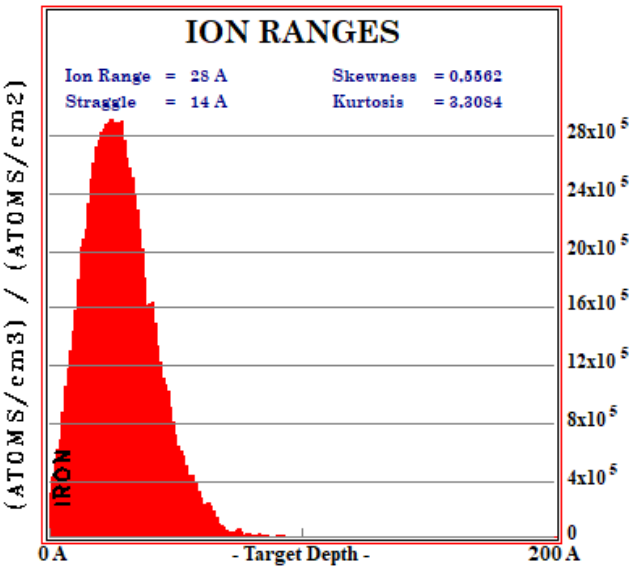

Figure 4. *Depth profile of the concentration of Kr^+ ions at an ion energy.*

As a function of Fe target depth, Figure 5 displays the energy

losses in eV/A^. displacement energy. As a result, the target atom vibrates and recoils, running out of energy to bounce off its location. The energy is finally released as phonons. The phonons of the recoiling target atoms are the main source of energy loss to the ions, as indicated by the red line at the bottom of the plot. The phonons of the recoiling atoms (Fe) are shown by the Gaussian, and the red line represents the energy loss to the phonons of the Kr^{+} ions. A flattened distribution peak near the surface is observed in simulations of the Krypton and Iron systems. The aforementioned suggests that the target's surface is where nuclear collisions lose energy.

The energy loss due to ionization is shown as a function of target depth in Figure 6. There are two different diagrams: one shows the energy loss of the recoiling target atoms and the other shows the electron energy loss of the incident ions. As can be seen in Figure 5, which displays the energy loss percentage, the incident ions lose relatively little energy (5.52%) to the target electrons, however the recoiling atoms deposit 17.62% of their energy, for a total energy loss of 23.14%. The projectile Kr+ ions transfer less energy than recoil atoms, according to the simulation results of the projectile ionization phenomena inside the Fe target. Kr has an overall ionization energy of 28 eV/A^ in the system under study. The lightest ion loses more energy in electronic form when the focus is on an iron target with incident energy set at 200 keV.

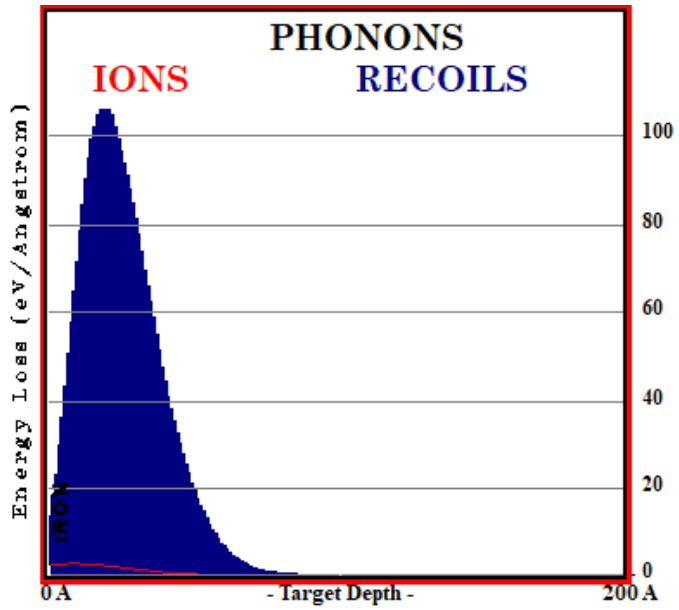

Figure 5. *The energy distribution of the phonons of the recoil atoms for different types of incident ions in Fe for an incident energy of 100 eV/A˚.*

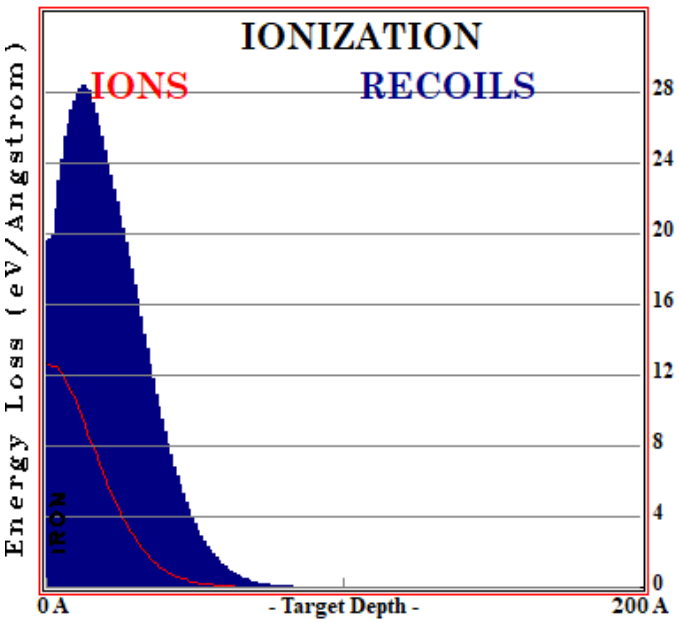

Figure 6. *The distribution of the ionization energy of incident ions (in red) and recoil atoms (in blue) for an incident energy of 28 eV/A˚ in Fe.*

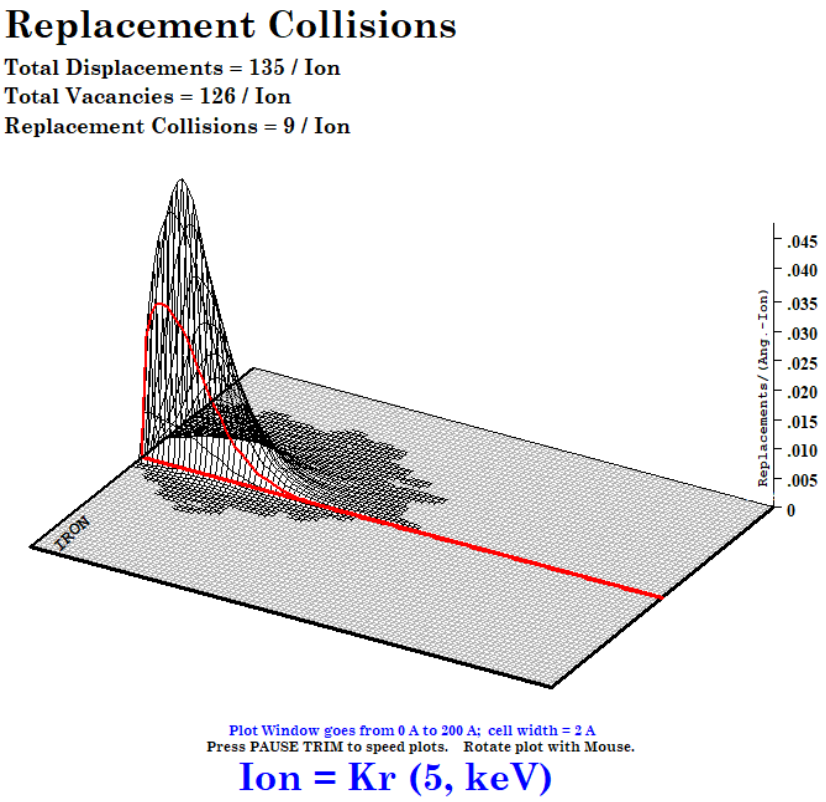

Figure 7. *Damage caused by collisions.*

The damage caused by collisions is displayed in Figure 7. Target movement as a whole is displayed by the upper curve. That is, the quantity of atoms extracted from their original location within the target. The empty spaces within the Fe target are depicted in the bottom curve that follows. This indicates that there are fewer unoccupied sites than displacements because the value is less than the intended displacement curve.

Crash replacements are represented by the lowest curve. When an incident atom loses nearly all of its energy during a displacement, it is unable to continue and falls into the space left by the retreating target atom. I.e., a target atom is taken out and reinserted into the lattice. Observing that the higher displacement curve is equal to the sum of the two lower curves is feasible. Thus: 134/ions of movements = 126/ions of vacancies + 9/ions of replacement collisions.

4. Conclusion

For the persistence of studying some fundamental thoughts of collision physics, the SRIM 2013 software in this episode is published. At the instant, experts in the field of ion implantation and sputtering operate it the most. This work shams some of the harm that can transpire when a solid iron target is struck by a 5 keV Kr^{+} ion, including atom dislocation and the creation of hollow sites. Edgewise with learning the sputtering phenomenon, nuclear and electronic energy losses are also evaluated. A few phenomena that arise through ion-matter interaction have been clarified by these few research and simulations.

The primary objective of this research is to calculate the energy deposition of helium ions in target organs and different entry layers, including as skin, water, soft tissue, muscular skeletal, and bone. The findings lead us to the following conclusions: Energy that fluctuates between 5 and 200 KeV is employed, operating the SRIM 2008 code, the program working for the computation,

Each energy beam's stopping power are calculated.

1) Z_2 and Z/A are comparable to the total stopping power.
2) The total (dE/dX) rises quickly at low energies, reaches a maximum, and then progressively reductions as energy increases.
3) The range of the heavy particles in the absorber material is may determined by using the stopping power.

The energy loss of acknowledged high energy particles is minimal (dE/dx) due to the unique energy dependence of the energy loss (or stopping power curve). Nevertheless, the energy loss increases when the particles slow down to energies that line up with the energy loss curve's peak. The largest energy loss happens at smaller depths for high commencement energies, and this reduces progressively as the absorption coefficient goes down towards lower energies. The range can be approximated, as body tissue is usually low Z material. The data from the SRIM code currently available agrees quite well with my fitting curves for the stopping power and range of alpha particles in water.

Abbreviations

Fe: Iron
Kr: Krypton
TS: ToF-SIMS
LSS: (Lindhard, Scharff, and Schiott)

Author Contributions

Mohamed Farjallah is the sole author. The author read and approved the final manuscript.

Conflicts of Interest

The authors declare no conflicts of interest.

References

[1] J. F. Ziegler at el, SRIM - The stopping and range of ions in matter, Nuclear Instruments and Methods in Physics Research B, 2010, 268, page 1818-1823. https://doi.org/10.1016/j.nimb.2010.02.091

[2] Berger, M. J, ESTAR, PSTAR, ASTAR, A PC package for calculating stopping powers and ranges of electrons, protons and helium ions, Version 2, International Atomic Energy Agency, nuclear data services, documentation series of the IAEA nuclear data section, 1993.

[3] National Research Council, Committee on the Biological Effects of Ionizing Radiation, Health Effects of Exposure to Low Levels of Ionizing Radiation, BEIR V, National Academy Press, Washington, D. C., 1990.

[4] Fred A. Mettler, Jr., M. D. and Arthur C. Upton, M. D. Medical Effects of Ionizing Radiation, Grune & Stratton, Inc., Orlando, Florida, 1995.

[5] Ahmed, S. N., physics and Engineering of Radiation Detection, Queen's University, Kingston, Ontario, 2007 118-120. https://doi.org/10.12691/ijp-5-3-5

[6] Y. H. Song, and Y. N. Wang, "Effect of ion-nucleus sizes on the electric stopping power for heavy ions in solids", Nucl. Instr. and Meth. in Phys. Res. B, 1998, 135, 124-127.

[7] W. Brandt, and M. Kitagawa, "Effective stopping-power charges of swift ions in condensed matter", Phys. Rev. B, 1982, 25, (9), 5631-5637. https://doi.org/10.1103/PhysRevB.25.5631

[8] L. E. Porter, "Further observations of projectile-z dependence in target parameters of modified Bethe-Bloch theory", Int. J. Quantum Chem. 2003, 95, (4-5), 504-511. https://doi.org/10.1002/qua.10589

[9] P. M. Echenique, R. M. Nieminen, J. C. Ashley, and R. Ritchie, "Nonlinear stopping power of an electron gas for slow ions", Phys. Rev. A, 1986, 33, (2), 897-904. https://doi.org/10.1103/PhysRevA.33.897

[10] J. F. Ziegler, Nucl. Instr. Meth. B, 2004, 1027, 219-220. https://doi.org/10.1016/j.nimb.2004.01.208

[11] J. F. Ziegler, "SRIM - the stopping and range of ions in matter", http://www.srim.org 2009

[12] A. Jablonski, C. J. Powell, and S. Tanuma, Surf. Interface Anal. 37, 861 (2005). https://doi.org/10.1002/sia.2104

[13] A. Jablonski, Prog. Surf. Sci, 2005, 79, (3). https://doi.org/10.1016/j.progsurf.2005.09.001

[14] A. Jablonski, F. Salvat, and C. J. Powell, J. Phys. Chem. Ref. Data, 2004, (33), 409. https://doi.org/10.1063/1.1595653

[15] F. Salvat, A. Jablonski, and C. J. Powell, Comput. Phys. Commun, 2005, 165, 157. https://doi.org/10.1016/j.cpc.2004.09.006

[16] ESTAR, PSTAR and ASTAR: Computer Codes for Calculating Stopping-Power and Range Tables for Electrons, Protons, and Helium Ions, Martin J. Berger* Ionizing Radiation Division National Institute of Standards and Technology Gaitherburg.

[17] Hunt, J. G., Dantas B. M., Azeredo, A. M. G. F. Visual Monte Carlo in-vivo in the CONRAD and IAEA Whole Body Counter Intercomparisons. In. Workshop on Uncertainty Assessment in Computational Dosimetry, Bologna, 2007

[18] J. C. Hsiao and K. Fong. Nature. 2004, 428 (6979), 218-220.

[19] T. Ozel, G. R. Bourret and C. a Mirkin. Nat Nanotechnol, 2015, 10 (4), 319-324. https://doi.org/10.1038/NNANO.2015.33

[20] S. V. Trukhanov, A. V. Trukhanov, V. A. Turchenko, A. V. Trukhanov, E. L. Trukhanova, D. I. Tishkevich, V. M. Ivanov, T. I. Zubar, M. Salem, V. G. Kostishyn, L. V. Panina, D. A. Vinnik and S. A. Gudkova. Ceram Int, 2018, 44, (1), 290-300. http://dx.doi.org/10.1016/j.ceramint

[21] C. R. Martin. Science, 1994, 266, (80), 1961-1966. https://doi.org/10.1126/science.266.5193.1961

[22] E. Y. Kaniukov, A. L. Kozlovsky, D. I. Shlimas, M. V. Zdorovets, D. V. Yakimchuk, E. E. Shumskaya and K. K. Kadyrzhanov. J Surf Investig X-ray, Synchrotron Neutron Tech, 2017, 11, (1), 270-275. https://doi.org/10.1134/S1027451017010281

[23] S. Y. Chou, P. R. Krauss and P. J. Renstrom. Science, 1996, 272, (5), (80), 85-87. http://dx.doi.org/10.1126/science.272.5258.85

[24] D. I. Tishkevich, S. S. Grabchikov, L. S. Tsybulskaya, V. S. Shendyukov, S. S. Perevoznikov, S. V. Trukhanov, E. L. Trukhanova, A. V. Trukhanov and D. A. Vinnik. J Alloys Compd, 2018, 735, 1943-1948.

[25] S. E. Demyanov, E. Y. Kaniukov, A. V. Petrov, E. K. Belonogov, E. A. Streltsov, D. K. Ivanov, Y. A. Ivanova, C. Trautmann, H. Terryn, M. Petrova, J. Ustarroz and V. Sivakov. J Surf Investig X-ray, Synchrotron Neutron Tech, 2014, 8, (4), 805-813. https://doi.org/10.1016/j.matpr.2018.12.085

[26] E. Kaniukov, A. Kozlovsky, D. Shlimas, D. Yakimchuk, M. Zdorovets and K. Kadyrzhanov. IOP Conf Ser Mater Sci Eng, 2016, 110, 12013. https://doi.org/10.1088/2053-1591/aab2bb

[27] N. A. Kalanda, G. G. Gorokh, M. V. Yarmolich, A. A. Lozovenko and E. Y. Kanyukov. Phys Solid State, 2016, 58, (2), 351-359. https://doi.org/10.1002/pssb.201900283

[28] A. Cultrera, L. Boarino, G. Amato and C. Lamberti. J Phys D Appl Phys, 2014, 47, 015102, 1-8.

[29] E. Kaniukov, A. Shumskaya, D. Yakimchuk, A. Kozlovskiy, A. Ibrayeva and M. Zdorovets. NANO 2016 Nanophysics, Nanomater Interface Stud Appl. 2017 (2017) 79-91.

[30] J. Liu, B. Liu, Z. Ni, Y. Deng, C. Zhong and W. Hu. Electrochim Acta, 2014, 150, 146-150.

[31] M. P. Proenca, C. T. Sousa, J. Ventura and J. P. Araújo. Magn Nano- Microwires Des Synth Prop Appl. 2015 (2015) Electrochemical Synthesis and Magnetism of Magnetic Nanotubes.; 2015.

[32] W. Li, L. Liao, X. Xiao, X. Zhao, Z. Dai, S. Guo, W. Wu, Y. Shi, J. Xu, F. Ren and C. Jiang. Nano Res., 2014, 7, (11), 1691-1698.

[33] A. Solanki, S. Choudhary, V. R. Satsangi, R. Shrivastav and S. Dass. J Alloys Compd, 2013, 561, 114-120. https://doi.org/10.1016/j.jallcom.2013.01.154

[34] I. P. Jain and G. Agarwal. Surf Sci Rep, 2011, 66, (3-4), 77-172. https://doi.org/10.1016/j.surfrep.2010.11.001

[35] S. Dhara. Crit Rev Solid State Mater Sci, 2007, 32, (1-2), 1-50.

[36] S. Panchal and R. P. Chauhan. Phys E Low-Dimensional Syst Nanostructures, (November 2016) (2017), 87, 37-43.

[37] R. P. Chauhan and P. Rana. Radiat Meas, 2015, 83, 43-46.

[38] Computer simulation of atomic-displacement cascades in solids in the binary-collisions approximation, Mark T. Robinson, lan M. Torrens, PHYSICAL Review B, 15 june 1974 (9) 12.

[39] J. F. Ziegler, J. Biersack, and U. Littmark, "The stopping and range of ions in matter, 1985, vol. 1", 1, Pergamon Press, New York.

[40] J. Ziegler, J. Biersack, and M. Ziegler, "Srim" the stopping and range of ions in matter, ion implantation press, 2008.

[41] J. Lindhard, M. Schar, and H. E. Schiøtt, Range concepts and heavy ion ranges, Munks-gaard Copenhagen, 1963.

[42] Junichiro Sameshima, Aya Takenaka, Yuichi Muraji, Shingo Ogawa, Masanobu Yoshikawa, Katsuaki Suganuma, Optimization of the depth resolution for profiling SiO/SiC interfaces by dual-beam TOF-SIMS combined with etching, Surf. Interface Anal, 2019, 51, 743. https://doi.org/10.18910/73559

[43] Pavel Andreevich Yunin, Yurii Nikolaevich Drozdov, Mikhail Nikolaevich Drozdov, A new approach to express ToF SIMS depth profiling, Surf. Interface Anal, 2015, 47, 771.

[44] Atsushi Murase, Takuya Mitsuoka, Mitsuhiro Tomita, Hisataka Takenaka, Hiromi Morita, An effect of measurement conditions on the depth resolution for low-energy dual-beam depth profiling using TOF-SIMS, Surf. Interface Anal, 2013, 45, 1261. https://doi.org/10.1002/sia.5266

[45] H. Faik-Etienne, Étude de l'implantation ionique dans les miroirs multicouches Mo/Si: application aux optiques diffractives, Thèse de doctorat, Institut National des Sciences Appliquées de Toulouse, 2005.